

Angular distribution of ${}^6\text{He}+p$ elastic scattering^{*}

LIU Xin(刘鑫)^{1,2} WANG You-Bao(王友宝)^{1,1)} LI Zhi-Hong(李志宏)¹
 JIN Sun-Jun(金孙均)¹ WANG Bao-Xiang(王宝祥)¹ LI Yun-Ju(李云居)¹
 LI Er-Tao(李二涛)¹ BAI Xi-Xiang(白希祥)¹ GUO Bing(郭冰)¹ SU Jun(苏俊)¹
 ZENG Sheng(曾晟)¹ YAN Sheng-Quan(颜胜权)¹ LIAN Gang(连钢)¹
 HUANG Wu-Zhen(黄悟真)¹ LIU Wei-Ping(柳卫平)¹

¹ Department of Nuclear Physics, China Institute of Atomic Energy (CIAE), Beijing 102413, China

² Institute of High Energy Physics, Chinese Academy of Sciences, Beijing 100049, China

Abstract: The angular distribution of ${}^1\text{H}({}^6\text{He},p){}^6\text{He}$ elastic scattering has been measured at $E_{c.m.} = 4.3$ MeV by using a thick-target inverse kinematic method. The experimental differential cross sections are reproduced by the distorted-wave Born approximation calculation utilizing the CH89 global optical potential parameter set. The real part of CH89 is reduced comparing with other potentials, which may be attributed to the couplings necessary for the weakly bound nuclei.

Key words: angular distribution, elastic scattering, thick-target method

PACS: 25.40.Cm, 24.10.Eq, 24.10.Ht **DOI:** 10.1088/1674-1137/36/8/006

1 Introduction

Nuclear reactions induced by radioactive ion beams (RIB) play a key role in exploiting the structure and interaction of short-lived exotic nuclei [1, 2]. The exotic behaviors found in nuclei with excessive neutrons include the neutron halo [3–5] and skin structure [6], the island of inversion [7–9], and the enhancement of the total-reaction cross section at sub-barrier energies [10–12]. These findings have largely enriched our knowledge and provide a stringent challenge to the nuclear models in a wider isospin freedom. In nuclear astrophysics, the reactions of RIBs with hydrogen or helium have to be emphasized, and the relevant interaction potential parameters are crucial ingredients in predicting the reaction rates [13].

A ${}^6\text{He}$ nucleus has a two-neutron halo structure, with a two-neutron separation energy of only 0.973 MeV. This interesting feature has attracted many investigations of the $({}^6\text{He}, {}^4\text{He})$ two-neutron transfer reaction for the di-neutron spectroscopic amplitude [14–17]. Special interest has been also shown in the interaction of ${}^6\text{He}$ with heavy elements, such

as ${}^{209}\text{Bi}$ [18–20], ${}^{238}\text{U}$ [21] and ${}^{208}\text{Pb}$ [22, 23]. For the ${}^6\text{He}+p$ entrance channel, Rogachev et al have studied the isobaric analog states of ${}^7\text{He}$ in ${}^7\text{Li}$ by the observation of the resonant yield of neutrons from the ${}^6\text{He}(p,n)$ reaction in coincidence with γ rays [24]. Radiative proton capture on ${}^6\text{He}$ was also investigated at $E({}^6\text{He})=40$ MeV, direct capture to the ground state and the first excited state of ${}^7\text{Li}$ were observed [25]. At the CIAE, a proton-neutron halo structure was found for the 3.563 MeV state in ${}^6\text{Li}$, by the angular distribution measurement of the ${}^1\text{H}({}^6\text{He}, {}^6\text{Li})n$ reaction [26]. As regards the elastic and inelastic scattering of ${}^6\text{He}+p$, several measurements have been carried out, mainly at the intermediate energy range [27–29]. As far as we know, there has been no angular distribution of the ${}^6\text{He}+p$ elastic scattering reported at low energy.

In the conventional thick-target inverse kinematic (TTIK) method, the incident beam is slowed down and stopped in the target while only the light reaction products escape from the target and are detected. The method is very useful and has been widely applied for the measurement of an excitation function

Received 2 November 2011

* Supported by National Natural Science Foundation of China (11021504, 10875173, 11175261, 10735100)

1) E-mail: ybwang@ciae.ac.cn

©2012 Chinese Physical Society and the Institute of High Energy Physics of the Chinese Academy of Sciences and the Institute of Modern Physics of the Chinese Academy of Sciences and IOP Publishing Ltd

in a large interval with a single RIB energy [30], owing to the precise reconstruction of the two-body reaction kinematics according to each laboratory angle [31]. This feature should also facilitate the simultaneous measurement of the angular distribution of multiple-energy points, especially when a large solid-angle detector array is used in the future. For this purpose, we extend the TTIK method to the measurement of the angular distribution of the ${}^1\text{H}({}^6\text{He}, \text{p}){}^6\text{He}$ elastic scattering at $E_{c.m.} = 4.3$ MeV.

2 Experiment

The experiment was carried out at the radioactive secondary beam facility of HI-13 tandem accelerator laboratory [32]. The ${}^6\text{He}$ ions were produced via the ${}^2\text{H}({}^7\text{Li}, {}^6\text{He}){}^3\text{He}$ reaction, with a 46 MeV ${}^7\text{Li}$ beam bombarding a deuterium gas cell of 1.5 atm pressure. The front and rear windows of the gas cell are Havar foils with the thickness of 1.9 mg/cm 2 . The secondary beam was separated and focused by the electro-magnetic dipole and quadrupole doublet on the beam line. Before bombarding the target, the ${}^6\text{He}$ secondary beam was collimated by a $\phi 9$ mm– $\phi 5$ mm collimator complex to limit the beam spot. During the experiment, the intensity of the secondary beam was approximately 1000 particles/s, and the purity of ${}^6\text{He}$ was better than 85%.

The schematic layout of the experimental setup is shown in Fig. 1. The ${}^6\text{He}$ secondary beam was identified and recorded with a 19.2 μm thin ORTEC silicon detector in front of the 79.2 mg/cm 2 $(\text{CH}_2)_n$ target. The energy of the ${}^6\text{He}$ ions impinging on the target was 36.4 MeV. A pure carbon target with the thickness of 104.2 mg/cm 2 was used to evaluate the background events from the carbon atoms in the $(\text{CH}_2)_n$ target. In this thick-target setup, the incident ${}^6\text{He}$ ions were fully stopped in the target. For the detection of the light recoil particles, we use a set of ΔE - E telescope which consists of a 67 μm double-sided silicon strip detector (DSSSD), and two multi-guard silicon quadrant (MSQ) detectors with thickness of 1001 μm and 982 μm , respectively. The DSSSD is comprised of 16 strips on the front side and 16 similar orthogonal strips on the back, thus providing two-dimension position information in a resolution of 3 mm \times 3mm. Both MSQ detectors are 2×2 arrays of independent active area, separated by a 0.1 mm wide cross gap. ΔE - E detectors are all 50 mm \times 50 mm of active area. In this experiment, a 14×14 pixel array in the central part of DSSSD was used which covers the laboratory angular range from

0° to 10° .

The total number of incident ${}^6\text{He}$ ions is approximately 1.31×10^8 for the $(\text{CH}_2)_n$ target runs, and 0.43×10^8 for the background measurement with the carbon target. The experimental proton spectrum was calibrated with proton beams scattering on Au of 440 $\mu\text{g}/\text{cm}^2$ at several energies, and with standard α sources of ${}^{148}\text{Gd}$ and ${}^{239}\text{Pu}$ - ${}^{241}\text{Am}$ mixed. A calibrated ΔE - E_t scatter plot is shown in Fig. 2, where ΔE is the energy loss of particles in the DSSSD, and E_t is the total energy that was detected.

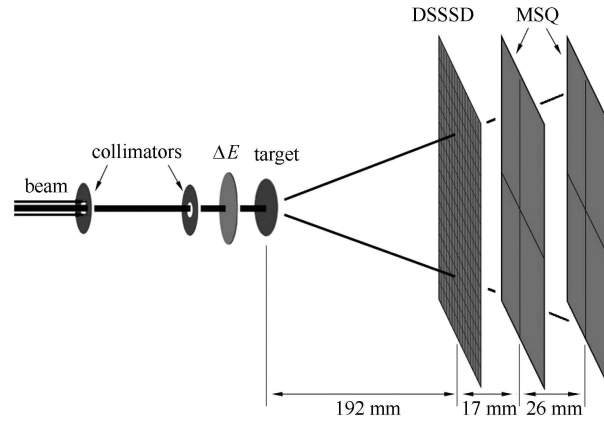


Fig. 1. Schematic layout of the experimental setup.

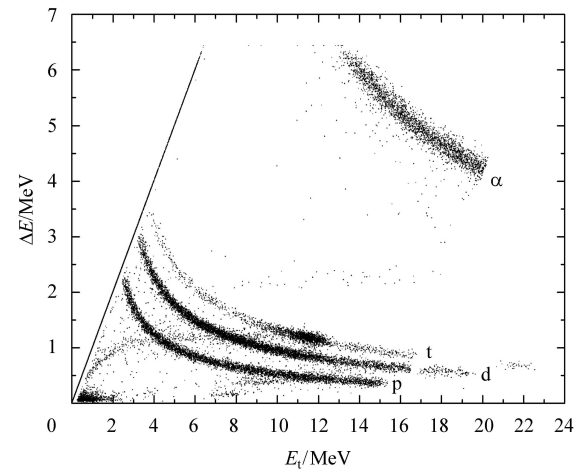


Fig. 2. The scatter plot of ΔE - E_t measured with the DSSSD and MSQ detectors.

3 Data analysis and result

Because of the thick-target effect, the proton energy spectrum is continuous at any individual angle corresponding to a certain range of experimental excitation function. At the reaction point, the $E_{c.m.}$ has a simple relation with the proton energy E_p as the

following:

$$E_{c.m.} = E_p \times \frac{m_p + m_A}{4m_A \cos^2 \theta_{lab}}, \quad (1)$$

where m_p and m_A are the masses of proton and ${}^6\text{He}$, respectively; $E_p = E_t + \Delta E_p$ which means the sum of detected proton energy plus the proton energy loss in the remaining $(\text{CH}_2)_n$ target after the reaction point.

As shown in our previous thick-target elastic resonance experiments [30, 31], one can reconstruct the reaction kinematics according to each laboratory angle, by taking into account the energy losses of ${}^6\text{He}$ and protons in the $(\text{CH}_2)_n$ target. Such kinds of kinematic reconstruction can be done with a Monte-Carlo simulation combining the reaction kinematics with the energy losses. As an example, the simulated $E_{c.m.}$ versus the detected proton total energy at $\theta_{lab} = 4.5^\circ$ is shown in Fig. 3. In the simulation, both the ${}^6\text{He}$ beam energy spread and angular divergence are considered, and the overall $E_{c.m.}$ resolution is about 30 keV, especially for $E_{c.m.} > 1.5$ MeV.

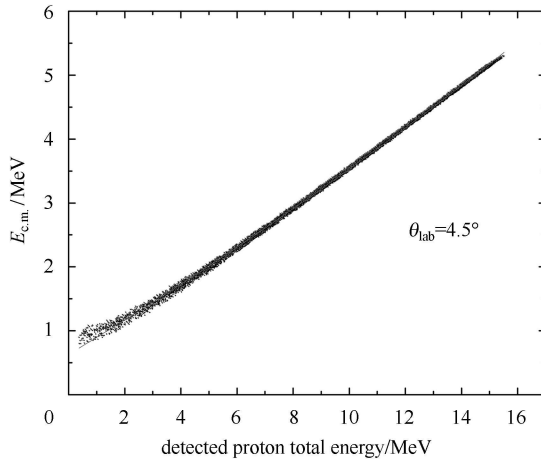


Fig. 3. The simulated $E_{c.m.}$ versus the detected proton total energy at $\theta_{lab} = 4.5^\circ$. The solid line indicates a fitting of the simulated data with a linear function. The behavior is close to linear at most parts of the detected energy region except for $E_{c.m.} < 1.5$ MeV where the deviation is obvious due to huge energy loss of the beam.

For most parts of the $E_{c.m.}$ range, the proton spectrum might be contaminated by the inelastic scattering to the first excited state of ${}^6\text{He}$ at 1.8 MeV, although it is unstable to the two-neutron emission immediately. Only the highest $E_{c.m.}$ part is free of inelastic scattering, therefore we chose an $E_{c.m.} = (4.30 \pm 0.16)$ MeV bin for analysis of the angular distribution of elastic scattering. The obtained angular distribution for ${}^1\text{H}({}^6\text{He}, p){}^6\text{He}$ elastic scattering is shown in Fig. 4. The corresponding effective

thickness of the $(\text{CH}_2)_n$ target is (6.6 ± 0.5) mg/cm². The errors of the differential cross section are mainly from the statistics, and from the uncertainties caused by the beam normalization (3%) and the simulation of the effective target thickness (8%). The angular uncertainties are also evaluated by including the beam spot size (0.3°), the angular divergence of the ${}^6\text{He}$ beam (0.2°), angular straggling generated when ${}^6\text{He}$ particles pass through the ΔE detector (0.22°) and $(\text{CH}_2)_n$ target (0.97°).

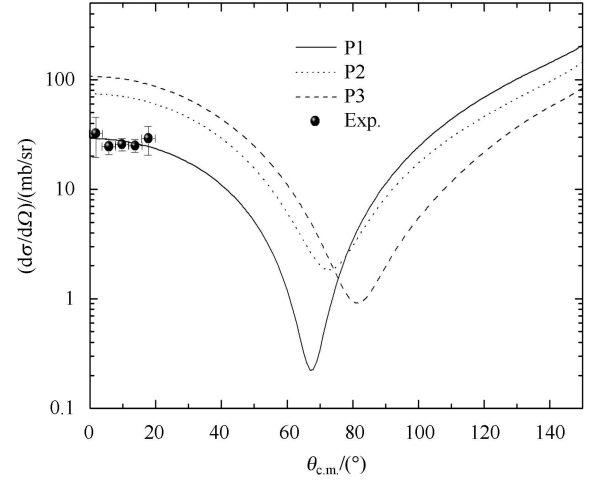


Fig. 4. Angular distribution of the ${}^1\text{H}({}^6\text{He}, p){}^6\text{He}$ elastic scattering at $E_{c.m.} = 4.3$ MeV. Details of the figure refer to section 4.

4 DWBA calculation and discussion

The experimental angular distribution was analyzed utilizing a distorted-wave Born approximation (DWBA) code, Ptolemy. A Woods-Saxon potential was used in the calculation, which can be expressed as

$$U(r) = -Vf(r, r_V, a_V) - iW_V f(r, r_W, a_W) - iW_S \frac{d}{dr} f(r, r_S, a_S) + V_{SO} f(r, r_{SO}, a_{SO}) + V_C, \quad (2)$$

where V and W_V are the depths of the real and imaginary parts, respectively; W_S is the depth of the surface term of the imaginary potential, and V_{SO} is the depth of the real part of the spin-orbit potential. The coulomb potential V_C and the form factor $f(r, r_i, a_i)$ take the following formula, respectively.

$$V_C = \frac{Z_P Z_T e^2}{2R_C} \left(3 - \frac{r^2}{R_C^2} \right), \quad r \leq R_C, \quad (3)$$

$$= \frac{Z_P Z_T e^2}{r}, \quad r > R_C,$$

$$f(r, r_i, a_i) = \left[1 + \exp\left(\frac{r - R_i}{a_i}\right) \right]^{-1}, \quad (4)$$

$$R_i = r_i(A_P^{1/3} + A_T^{1/3}), \quad i = V, W, S, SO, \quad (5)$$

where Z_P , Z_T , and A_P , A_T are the charge numbers and masses of the projectile and target, respectively.

Three sets of global potential parameters are applied in the DWBA calculation, as listed in Table 1. It is clear that only P1 reproduces the experimental differential cross sections, while P2 and P3 fail with much higher values as shown in Fig. 4. The P1 parameter set was developed by Varner et al. [33], and is usually called Chapel-Hill 89 (CH89). It is based on the understanding of the basis of the optical potential, such as the folding model and nuclear matter approaches instead of the determination of optical-model potentials phenomenologically. The potential parameters were obtained by fitting a large amount of differential cross sections for proton and neutron elastic scattering on nuclei in the energy domain of 10–65 MeV. Previously, the CH89 was proved to give a better fitting to the experimental data, and has been widely used with success in analyzing the proton elastic scattering on light nuclei [36].

Table 1. Optical potential parameters used in the DWBA calculation. The potentials have a standard Wood-Saxon form, V and W are in MeV, r and a are in fm.

set No.	P1	P2	P3
V	56.01	60	86.88
r_V	1.126	1.25	1.08
a_V	0.69	0.65	0.68
W_V	0.993		0.46
r_W	1.099		1.08
a_W	0.69		0.68
V_S	15.46	13.5	9.14
r_S	1.099	1.25	1.31
a_S	0.69	0.47	0.52
V_{SO}	5.9	7.5	5.63
r_{SO}	0.68	1.25	0.59
a_{SO}	0.63	0.47	0.83
r_C	1.30	1.25	1.25
Ref.	[33]	[34]	[35]

In the intermediate energy elastic scattering of ${}^6\text{He}+\text{p}$, it was found that the CH89 potential gives also very good results compared with the microscopic

optical model approach [27–29]. Although CH89 does not implicitly include any density distribution, the potentials can well reproduce the intermediate energy experimental data provided that the real part was reduced or the imaginary part enhanced. This was attributed to the couplings necessary for the weakly bound nuclei, which could be related to a dynamic polarization potential generated in the break-up process. The potential is significant especially when the momentum transfer is larger than the typical internal momentum of the halo neutrons. Such a potential is usually presented as a positive real part resulting in a decrease of the total real potential [37], or a negative imaginary part which increases the total imaginary potential [38]. When comparing P1 with P2 and P3 used here, the real part of P1 is indeed the smallest, which might indicate that the couplings with the break-up process is not negligible even at the low energy domain.

5 Summary

The angular distribution of the ${}^6\text{He}+\text{p}$ elastic scattering is measured at $E_{\text{c.m.}} = 4.3$ MeV with a TTIK method. The experimental angular distribution is analyzed by DWBA calculations utilizing several sets of the global optical potentials, where only the CH89 potential reproduces the experimental differential cross sections. Since the experiment was initially motivated for the measurement of the excitation function of ${}^6\text{He}+\text{p}$, only five data points at forward angles are obtained. However, one can see that the experimental differential cross sections impose important regulations on the depths of the optical potentials. This experiment also shows that the angular distribution of the proton elastic scattering induced by RIBs can be obtained via a TTIK method. By using a large solid-angle detector array in the future, the TTIK method can be a powerful multi-purpose tool with its analyzing power of the excitation function and angular distributions simultaneously.

The authors would like to thank the technical staff of the HI-13 Tandem Accelerator Laboratory for preparing the targets and the smooth operation throughout the experiment.

References

- 1 Keeley N, Alamanos N, Kemper K W et al. *Prog. Part. Nucl. Phys.*, 2009, **63**: 396–477
- 2 Tanihata I. *Nucl. Instrum. Methods B*, 2008, **266**: 4067–4073
- 3 Tanihata I, Hamagaki H, Hashimoto O et al. *Phys. Rev. Lett.*, 1985, **55**: 2676
- 4 Jonson B. *Phys. Rep.*, 2004, **389**: 1–59
- 5 Tanaka K, Yamaguchi T, Suzuki T et al. *Phys. Rev. Lett.*, 2010, **104**: 062701
- 6 Kanungo R, Prochazka A, Horiuchi W et al. *Phys. Rev. C*, 2011, **83**: 021302(R)
- 7 Caurier E, Martinez-Pinedo G, Nowacki F et al. *Rev. Mod. Phys.*, 2005, **77**: 2
- 8 Nakamura T, Kobayashi N, Kondo Y et al. *Phys. Rev. Lett.*, 2009, **103**: 262501
- 9 Lenzi S M, Nowachi F, Poves A et al. *Phys. Rev. C*, 2010, **82**: 054301
- 10 DeYoung P A, Mears P J, Kolata J J et al. *Phys. Rev. C*, 2005, **71**: 051601(R)
- 11 Di Pietro A, Randisi G, Scuderi V et al. *Phys. Rev. Lett.*, 2010, **105**: 022701
- 12 Alcorta M, Rehm K E, Back B B et al. *Phys. Rev. Lett.*, 2011, **106**: 172701
- 13 Bertulani C A, Gade A. *Phys. Rep.*, 2010, **485**: 195–259
- 14 Ter-Akopian G M, Rodin A M, Fomichev A S et al. *Phys. Lett B*, 1998, **426**: 251–256
- 15 Raabe R, Piechaczek A, Andreyev A et al. *Phys. Lett. B*, 1999, **458**: 1
- 16 Raabe R, Andreyev A, Huyse M et al. *Phys. Rev. C*, 2003, **67**: 044602
- 17 Khoa D T, Oertzen W V. *Phys. Lett. B*, 2004, **595**: 193–201
- 18 Kolata J J, Guimaraes V, Peterson D et al. *Phys. Rev. Lett.*, 1998, **81**: 4580
- 19 Bychowski J P, DeYoung P A, Hildore B B et al. *Phys. Lett. B*, 2004, **596**: 26–31
- 20 Aguilera E F, Kolata J J, Nunes F M et al. *Phys. Rev. Lett.*, 2000, **84**: 5058
- 21 Trotta M, Sida J L, Alamanos N et al. *Phys. Rev. Lett.*, 2000, **84**: 2342
- 22 Kakuee O R, Alvarez M A G, Andres M V et al. *Nucl. Phys. A*, 2006, **765**: 294–306
- 23 Sánchez-Benítez A M, Escrig D, Alvarez M A G et al. *Nucl. Phys. A*, 2008, **803**: 30–45
- 24 Rogachev G V, Boutachkov P, Aprahamian A et al. *Phys. Rev. Lett.*, 2004, **92**: 232502
- 25 Sauvan E, Marques F M, Wilschut H W et al. *Phys. Rev. Lett.*, 2001, **87**: 042501
- 26 LI Z H, LIU W P, BAI X X et al. *Phys. Lett. B*, 2002, **527**: 50–54
- 27 Lapoux V, Alamanos N, Auger F et al. *Phys. Lett. B*, 2001, **517**: 18–24
- 28 Lagoyannis A, Auger F, Musumarra A et al. *Phys. Lett. B*, 2001, **518**: 27–33
- 29 Stepantsov S V, Bogdanov D D, Fomichev A D et al. *Phys. Lett. B*, 2002, **542**: 35–42
- 30 WANG Y B, WANG B X, QIN X et al. *Phys. Rev. C*, 2008, **77**: 044304
- 31 WANG Y B, QIN X, WANG B X et al. *Chin. Phys. C (HEP & NP)*, 2009, **33**: 181
- 32 BAI X X, LIU W P, QIN J C et al. *Nucl. Phys. A*, 1995, **588**: 273c
- 33 Varner R L, Thompson W J, McCabe T L et al. *Phys. Rep.*, 1991, **201**: 57–119
- 34 Perey C M, Perey F G. *At. Data Nucl. Data Tables*, 1976, **17**: 1
- 35 Koning A J, Delaroche J P. *Nucl. Phys. A*, 2003, **713**: 231
- 36 LIU X D. PhD thesis, Michigan State University, 2005
- 37 Hirabayashi Y, Sakuragi Y. *Phys. Lett. B*, 1991, **258**: 11
- 38 Hirenzaki S, Toki H, Tanihata I. *Nucl. Phys. A*, 1993, **552**: 57–65